SANDIA REPORT
SAND2012-8498
Unlimited Release
Printed October 2012

Quantum Enhanced Technologies

Akash Rakholia, Hayden McGuinness, Grant Biedermann

Prepared by
Sandia National Laboratories
Albuquerque, New Mexico 87185 and Livermore, California 94550

Sandia National Laboratories is a multi-program laboratory managed and operated by Sandia Corporation, a wholly owned subsidiary of Lockheed Martin Corporation, for the U.S. Department of Energy's National Nuclear Security Administration under contract DE-AC04-94AL85000.

Approved for public release; further dissemination unlimited.

Sandia National Laboratories

Issued by Sandia National Laboratories, operated for the United States Department of Energy by Sandia Corporation.

NOTICE: This report was prepared as an account of work sponsored by an agency of the United States Government. Neither the United States Government, nor any agency thereof, nor any of their employees, nor any of their contractors, subcontractors, or their employees, make any warranty, express or implied, or assume any legal liability or responsibility for the accuracy, completeness, or usefulness of any information, apparatus, product, or process disclosed, or represent that its use would not infringe privately owned rights. Reference herein to any specific commercial product, process, or service by trade name, trademark, manufacturer, or otherwise, does not necessarily constitute or imply its endorsement, recommendation, or favoring by the United States Government, any agency thereof, or any of their contractors or subcontractors. The views and opinions expressed herein do not necessarily state or reflect those of the United States Government, any agency thereof, or any of their contractors.

Printed in the United States of America. This report has been reproduced directly from the best available copy.

Available to DOE and DOE contractors from
U.S. Department of Energy
Office of Scientific and Technical Information
P.O. Box 62
Oak Ridge, TN 37831

Telephone: (865) 576-8401
Facsimile: (865) 576-5728
E-Mail: reports@adonis.osti.gov
Online ordering: http://www.osti.gov/bridge

Available to the public from
U.S. Department of Commerce
National Technical Information Service
5285 Port Royal Rd.
Springfield, VA 22161

Telephone: (800) 553-6847
Facsimile: (703) 605-6900
E-Mail: orders@ntis.fedworld.gov
Online order: http://www.ntis.gov/help/ordermethods.asp?loc=7-4-0#online

SAND2012-8498
Unlimited Release
Printed October 2012

Quantum Enhanced Technologies

Akash Rakholia, Hayden McGuinness, Grant Biedermann
Photonic Microsystems
Sandia National Laboratories
P.O. Box 5800
Albuquerque, New Mexico 87185-MS1082

Abstract

Quantum effects have a wide variety of applications in computation, communication, and metrology. To explore practical quantum enhanced technologies, we are investigating quantum metrology in neutral atom systems, such as inertial sensors and clocks, which could revolutionize the field of precision navigation. The lower noise boundary on measurements of a two-level quantum system is given by the standard quantum limit (SQL). This limits the signal-to-noise ratio (SNR) to SNR = $\sqrt{N}$ where N is the number of atoms. Using Quantum Non-Demolition techniques (QND), it has been demonstrated that one can surpass the SQL, with the ultimate limit given by the Heisenberg Limit of SNR = N. For many implementations, this limit corresponds to an improvement by several orders of magnitude. However, achieving even the SQL is difficult in practical systems. To realize the gains of quantum enhanced metrology one must first realize high fidelity measurements of quantum systems. This fidelity is often limited by sources of technical noise in the system which must be characterized and mitigated.

In this report we attempt to experimentally reach the SQL in a system of laser-cooled Rubidium 87 atoms. Atomic transitions were induced through microwave radiation and the stimulated Raman interaction. We characterize the various sources of noise that hinder the achievement of the SQL and compare our measurements to theoretical models that take these impediments into consideration. Additionally, we survey the literature for spin-squeezing techniques which allow for Heisenberg-limited measurements in similar cold-atom systems. Our investigation confirmed the difficulty of achieving even moderate amounts of squeezing for a metrologically relevant quantity. However, spin squeezing could prove to be an important technique for atom interferometry if substantial improvements in implementation are made. This work is done in collaboration with the University of New Mexico.

CONTENTS

1. Introduction 7

2. Microwave Experiments 7
   2.1. Rubidium 87 MOT Experiment 7
      2.1.1 Determining Shot Noise Limit 8
      2.1.2 Recapture 9
      2.1.3 Results 9
   2.2 Rubidium 87 Vapor Cell 11

3. Stimulated Raman Transition Theory 13
   3.1 Pulse Efficiency Limitations 14
   3.2 Enhanced Sensitivity 15
   3.3 Raman Fringes 17

4. Theoritical Exploration of Spin Squeezing 19
   4.1 Theory 19
   4.2 Application to Atom Interferometry 20
      4.2.1 Spin Squeezing by Atomic Interactions and Atom-Light Mapping 20
      4.2.2 Spin Squeezing by Quantum Non-Demolition Measurement 22

5. Conclusions 26

6. References 28

Distribution 29

FIGURES

Figure 1. Left: Energy level diagram of Rb 87. Right: The experimental setup used to trap ~10^5 Rb 87 atoms and cool them to 5 μK. Shown in this image are the trapping beams, pumping beams, detector, and microwave horn used to prepare, generate, and observe transitions between the hyperfine ground states of Rb 87. 8

Figure 2. Microwave SNR vs Interrogation time. The lack of magnetic shielding results in a strong decay of SNR for longer interrogation times. SNR is maintained with the use of a magnetic shield. 10

Figure 3. Simulation of microwave SNR to account for magnetic field fluctuations and the second-order Zeeman effect. 11

Figure 4. Experimental setup used to test a variety of vapor cells. The experiment consists of probe and repump beams, along with a microwave horn. The cell is housed in a temperature-controlled chamber. 11

Figure 5. Microwave fringes in a vapor cell with paraffin coating. Coherence of the atoms is maintained over longer interrogation times, despite collisions with walls. 12

Figure 6. Left: A pair of laser beams detuned by the hyperfine resonance, ν_{hf}, couples the ground states of the atom, forming a stimulated Raman Transition. Right: A $\pi/2 - \pi - \pi/2$ pulse sequence with Raman beams forms an interferometer in space. 13

Figure 7. Sample of experimental results for Raman Rabi flopping. The observed π pulse efficiency is 70%..... 14
Figure 8. Simulated Raman Rabi flopping. Left: 30 μK atomic sample. Right: Hypothetical 0K. Atomic sample is half the diameter of the Raman beam. Bottom: A combination of the two systematic effects..... 15
Figure 9. Plot of sensitivity vs number of additional pulses. For each π pulse efficiency, there is an optimal number of pulses..... 16
Figure 10. Top: Optimal number of pulses for a given efficiency. Bottom: Resulting sensitivity, given efficiency Ɛ, using the number of pulses derived from top figure..... 16
Figure 11. Fringes from a Doppler-sensitive interferometer. The phase noise corresponds to an SNR of 30. 17
Figure 12. Left: Spin coherent state in a quantum-limited regime. Right: Coherent state squeezed along J_y..... 19
Figure 13: From [9]. (a) Evolution of an input squeezed state with an interferometer sequence. The squeezing initially produces reduced error in the $\boldsymbol{Jy}$ component, but this is transferred to the $\boldsymbol{Jz}$ component for measurement. (b) Fringes for the squeezed (red) and non-squeezed (blue) input states. (c) Uncertainties in the phases for squeezed and non-squeezed states mid-fringe. 21
Figure 14: From [10]. Experimental setup for mapping a squeezed light state onto an ensemble of cold Cs atoms. Coherent and squeezed light is incident on the ensemble, creating a spin entangled, and spin squeezed, state. The component of the ensemble spin which is squeezed is measured via probe beam and lock-in detection methods. 22
Figure 15. From [13]. Left: Interferometer used to detect phase shifts in the probe beam. Right: Energy level diagram of the two-color probe beam..... 22
Figure 16. From [13]. Experimental sequence used to surpass the SQL by QND measurement.23
Figure 17. Simulation used to model recapture efficiency vs time of flight from a dipole trap. Parameters used were ω_0 = 20 μm, T = 1 μK. 24
Figure 18. Optimal sensitivity of an atom interferometer out of a dipole trap using SQL limited detection vs Heisenberg limited detection. 25

NOMENCLATURE

MOT	Magneto Optical Trap
SNR	Signal to Noise Ratio
SQL	Standard Quantum Limit
HL	Heisenberg Limit
SNL	Sandia National Laboratories
QND	Quantum Non-Demolition
Rb	Rubidium
Cs	Cesium
BEC	Bose-Einstein Condensate

1. INTRODUCTION

Enhancements from quantum metrology may be applied to two-level systems which are known for their exceptional performance in inertial sensing, clocks, metrology, and spectroscopy. As a specific example, accurate inertial measurements are essential in a region where GPS may be denied. The sensitivity of such systems is usually limited by the standard quantum limit (SQL), which places an upper bound of SNR = $\sqrt{N}$, where N is the number of atoms in an ensemble. Using advanced techniques such as spin squeezing, it is possible to derive another bound known as the Heisenberg limit where SNR = N. For a system of ~10^5 atoms, this limit represents an improvement by several orders of magnitude. However, achieving such a bound is difficult in practice. The ultimate performance of such technology requires understanding sources of noise and mitigating them to reach the Heisenberg limit.

In this work we identify, characterize, and mitigate sample sources of noise to work towards a Heisenberg-limited system for quantum metrology. To this end, initial experiments were carried out with microwave transitions in various systems to work towards the SQL. Secondly, we theoretically analyzed the limiting factors in an atom interferometer system, another promising application of quantum metrology. Finally, we carried out an analysis of surpassing the SQL in a novel atom interferometer system.

2. MICROWAVE EXPERIMENTS

Preliminary investigations focused on observing microwave coherence in a system of cold atoms trapped in a magneto optical trap [1]. Microwave transitions on these systems have been studied thoroughly in the past. Observing such a system provides a reference with which we can investigate improvements, as well as alternative systems.

Rubidium 87 was chosen for these investigations due to the smaller hyperfine manifold (d = 8) as opposed to cesium (d = 16). We achieved nearly shot noise limited sensitivity in an ensemble of 10^5 cold atoms trapped in a MOT. One unique feature of the system is a high data rate (~100 Hz) using atom recapture, which recycles atoms shot-to-shot.

2.1. Rubidium 87 MOT Experiment

We used an existing 87Rb MOT system to carry out microwave investigations (see Fig. 1). Approximately 10^5 87Rb are cooled to 5 μK and released in free fall. Atoms are pumped with linearly polarized D_2 light on the F=2 → F'=2 transition, resulting in 43% of the atoms being pumped into the magnetic field insensitive $|F = 1, m_f = 0\rangle$ state. Atoms are then interrogated with a microwave pulse sequence, and the population in $|F = 2\rangle$ as well as the total atom number are recorded by fluorescence detection.

By sweeping the duration of a microwave pulse tuned to the hyperfine resonance, we can coherently transfer population between the ground state levels. A "π" pulse transfers full population to the other state, while a "π/2" pulse generates an equal superposition of population in the ground state levels.

We can create a microwave clock by using a $\pi/2 - \pi - \pi/2$ pulse sequence, where the pulses are separated by some interrogation time T. The phase sensitivity of this clock is given by

$$=,$$

where N is the number of atoms in the sample. We refer to as the SNR, and SNR is referred to as the standard quantum limit (SQL).

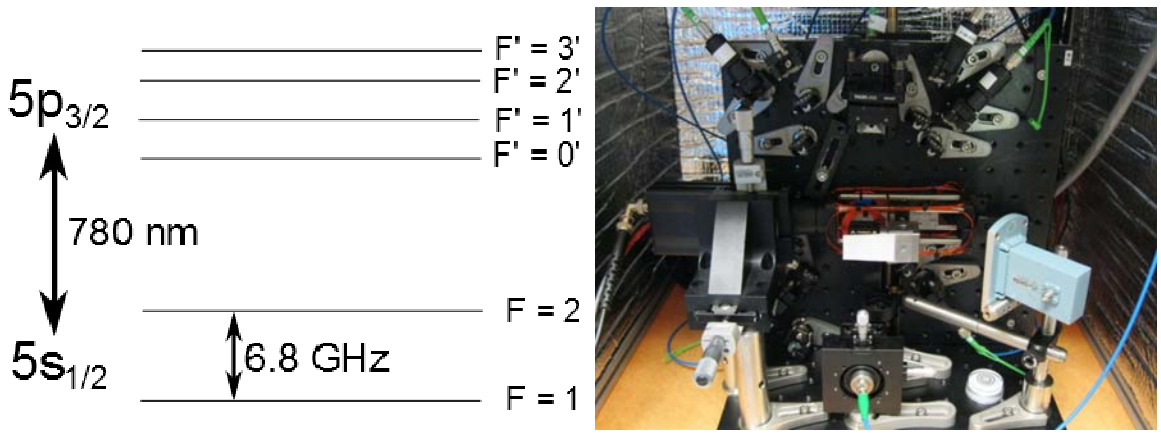

Figure 1. Left: Energy level diagram of 87Rb. Right: The experimental setup used to trap ~10^5 87Rb atoms and cool them to 5 μK. Shown in this image are the trapping beams, pumping beams, detector, and microwave horn used to prepare, generate, and observe transitions between the hyperfine ground states of 87Rb.

2.1.1 Determining Shot Noise Limit

To experimentally determine the SNR it is essential to measure the participating number of atoms. For experiments involving macroscopic numbers of laser cooled atoms there are several possible techniques for estimating atom number with reasonable accuracy. One method known as fluorescence detection measures photons scattered off of atoms from a probe laser beam. Another method known as absorption detection measures the loss of photons from the probe beam as a result of scattering off of the atomic ensemble. For all experiments presented in this report we use fluorescence detection, which is particularly convenient for our setup due to second order sensitivity to probe intensity given a sufficiently high saturation intensity of the probe beam.

Fluorescence detection can be summarized qualitatively as follows. The atom ensemble is prepared in one of the hyperfine ground states with high efficiency through various light-atom interactions [2]. A beam of near resonant detection light with $1/e^2$ waist ρ, which is significantly larger than the ensemble cloud diameter, and power is incident upon the ensemble. The atoms scatter the light isotropically at a rate depending on the specific atom species, energy level, light intensity, and polarization. Each atom scatters at a rate independent of all other atoms, so the total light scattered is proportional to the number of prepared atoms. Hence by collecting some know fraction of the scattered light, the total atom number in the ensemble can be measured.

Our experiments detect 87Rb atoms along the D_2 transition at $\lambda = 780.24$ nanometers (nm). The atomic scattering rate of this state from low power detection light detuned by a small amount δ is given by,

$$\xi = \frac{s_0\gamma/2}{1 + s_0 + (\delta/\gamma)^2}$$

where $s_0 = I/I_s$ is the saturation parameter, $I = P/\pi\rho^2$ is the detection beam intensity, $I_s = \frac{\pi hc\gamma}{3\lambda^3} = 1.67$ mW/cm^2 is the saturation intensity for this 87Rb transition, $\gamma/2\pi = 6.06$ MHz is the transition linewidth, h is Planck 's constant, and c is the speed of light. We detect the light with a Hamumatsu C5460-01 avalanche photo diode (APD) and capture approximately $\varepsilon = 0.012$ fraction of the scattered light. The power from the scattered photons incident on the APD from each atom is

$$P_a = \frac{hc\xi\varepsilon}{\lambda}.$$

With the APD gain measured to be $\alpha = 8.7 * 10^7$V/W and a signal measurement in volts of S, the total atom number of the ensemble is measured to be

$$N_{tot} = \frac{S}{\alpha * P_a}.$$

From this equation we can calculate the quantum limited, atom shot-noise SNR limit of $\sqrt{N_{tot}}$. Various values of P and ρ were used in the measurements.

2.1.2 Recapture

Typically MOT based atomic physics experiments suffer from poor bandwidth due to the need to load the MOT from vapor between shots, a process which takes ~1 s. As a side project, we investigated the efficiency of recapturing atoms from the previous shot before they fully dissipate into vapor. Our initial experiments achieved a mere 50% recapture efficiency, limited primarily by the switching time of our magnetic field coils, which was approximately 1 ms. By using different current controllers and smaller coils, we were able to reduce this to 50 μs.

After optimizing timing for the experiment, we achieved a high data rate on the order of 100 Hz with ~10^5 atoms, far more than would be possible loading directly from vapor [3]. Using this technique, ~90% of the atoms are recaptured for the next shot of the experiment. As an example, with a 100 Hz cycle we trapped 2×10^5 atoms and recaptured 92% of them in 1.7 ms. Loading this many atoms from vapor would have taken greater than 20 ms, which is slower than the bandwidth of our experiment.

2.1.3 Results

For 10^5 atoms as measured with the technique discussed above, the SQL places the maximum SNR at 316. Initial experiments were able to achieve 250 SNR with 0.25 ms of interrogation time. However, the SNR significantly diminished for higher interrogation times (Fig. 2).

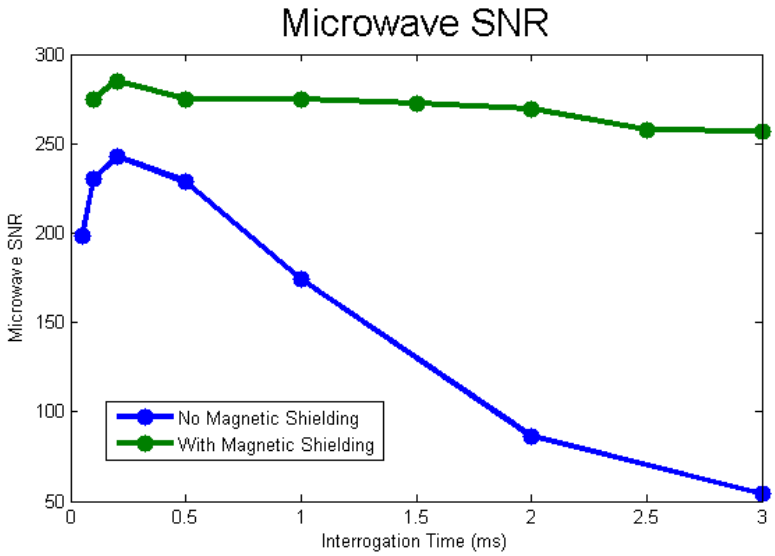

Figure 2. Microwave SNR vs Interrogation time. The lack of magnetic shielding results in a strong decay of SNR for longer interrogation times. SNR is maintained with the use of a magnetic shield.

Despite using the magnetically insensitive $m_F = 0$ state, the system is still sensitive to perturbations from the second-order Zeeman shift, given by $\delta\nu = (575.15\ Hz/G^2)B^2$. Fluctuations from the ambient magnetic field were measured to be 20 mG Pk-Pk at 60 Hz, with a DC field of 1.5 G for the quantization axis. A simulation of the SNR was run assuming a starting SNR of 300 and these field parameters. Results are shown in Fig. 3. The simulation agrees qualitatively with the experimental results from Fig. 2, indicating that the second-order Zeeman shift is a likely cause of the loss of contrast at higher interrogation times.

By placing the apparatus inside a permeable (mu-metal) magnetic shield, the ambient magnetic field was lowered to less than 1 mG. The microwave experiment was repeated and achieved 280 SNR, and maintained 250 SNR with up to 3 ms of interrogation (Fig. 2). This corresponds to a magnetic field noise of 0.2 mG, an improvement by two orders of magnitude.

If the system was purely limited by the Heisenberg limit, the corresponding SNR would be approximately 10^5. However, the dominating source of noise would still be from the magnetic field, and would limit us to an SNR of 450. Therefore, in order to realize the Heisenberg limit, it would be necessary to further suppress the field noise by another two orders of magnitude or reduce the second-order field sensitivity by lowering the DC bias field. The former is can be accomplished through the use of additional magnetic shielding.

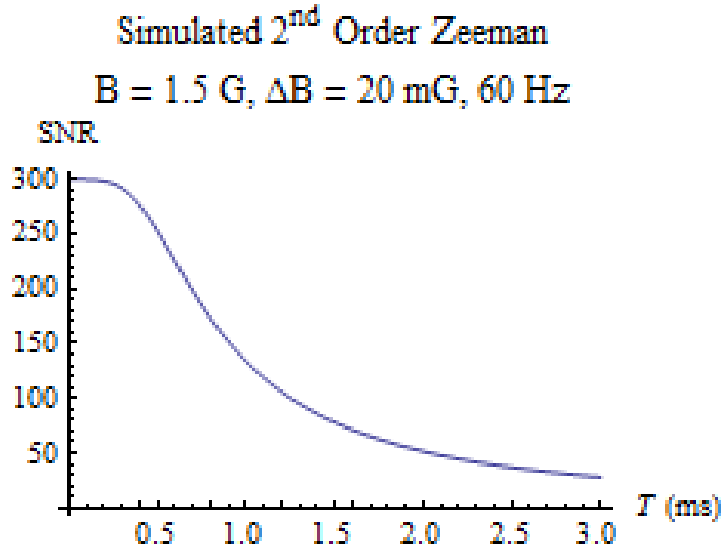

Figure 3. Simulation of microwave SNR to account for magnetic field fluctuations and the second-order Zeeman effect.

2.2 Rubidium 87 Vapor Cell

Cold atom systems introduce additional complexity due to the need for cooling and repumping lasers. An alternative approach uses a hot vapor cell, which is a much simpler system and is far more scalable. However, when atoms bounce off the wall of such a cell, the state of the atom no longer maintains spin coherence. One solution is to use an anti-relaxation coating, such as paraffin [4].

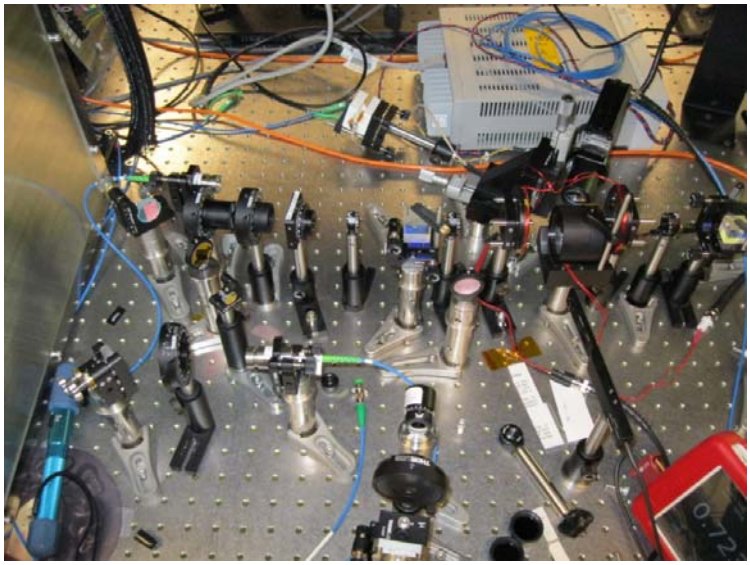

Figure 4. Experimental setup used to test a variety of vapor cells. The experiment consists of probe and repump beams, along with a microwave horn. The cell is housed in a temperature-controlled chamber.

We set up an apparatus to investigate microwave transitions with a variety of cells, coatings, and atomic densities (Fig. 4). For the primary experiment, we used a quartz cell with a volume of ~1 cm^3 and walls coated with paraffin. At 50°C, half of the atoms collide with the wall after 15 μs. This theoretically limits the interrogation time to $T \sim 10$ μs. However, the paraffin coating significantly increases this by maintaining atomic coherence after a wall bounce.

Atoms were pumped into the F=1 manifold using the probe beam resonant on F=2 → F'=3 transition. They were then interrogated with a $\pi/2 - \pi - \pi/2$ microwave pulse sequence, and T was varied from 10 μs to 160 μs. The population of atoms in F = 2 was detected by absorption measurement through a low intensity probe beam.

Fig. 5 shows experimental data for fringe scans at various values of T. It is evident that microwave coherence is maintained at least 10 times longer than we would expect without relaxation coating. These un-optimized scans, which involved fluctuating probe intensity and low atom number, have an SNR ranging from 70 to 50.

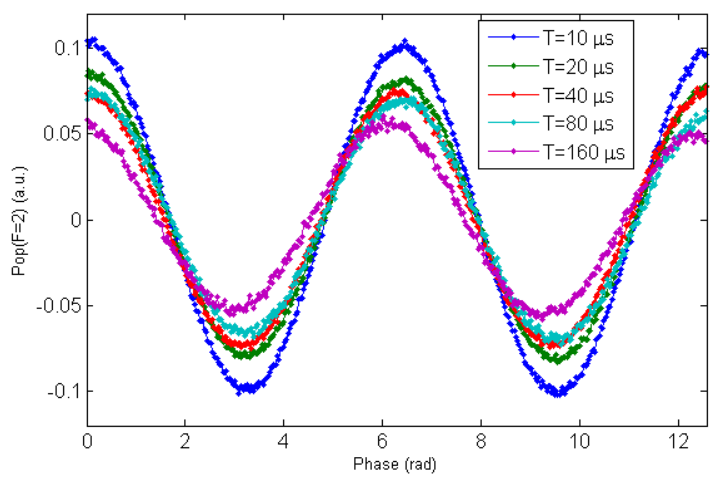

Figure 5. Microwave fringes in a vapor cell with paraffin coating. Coherence of the atoms is maintained over longer interrogation times, despite collisions with walls.

For a calculation of the potential SNR, we will assume a room-temperature (T = 300 K) cell with a volume of 1 cm^3, which closely approximates the experimental setup. Assuming a D_2 probe transition limited by the natural linewidth of the transition ($\Gamma = 2\pi \times 6.066$ MHz), the probe beam addresses approximately 1% of room-temperature atoms. Calculating the atom number from the partial pressure of 87Rb at room temperature (3×10^{-7} torr), we find 10^{10} atoms occupying the volume of the cell. Accounting for the number addressed by the probe, we have N = 10^8. At the SQL, we should be able to achieve an SNR of 10,000. Noise limitations due to our detection and pumping methods severely restricted the SNR of our system.

3. STIMULATED RAMAN TRANSITION THEORY

Certain classes of metrological experiments rely on applying large photon recoils to the atom in order to manipulate the internal and external state of the atom simultaneously [5]. The sensitivity of these experiments scales as the area enclosed by an interferometer, which in turn depends on the velocity recoil applied to the atoms. The velocity recoil from a microwave photon is given by $\hbar k$, where $k \sim 1$ cm^{-1}. By using an optical transition, the recoil is now given by $\hbar k$, where $k \sim 10^5$ cm^{-1}, five orders of magnitude higher. However, optical excited states are short-lived. One solution is to use a pair of Raman beams detuned from each other by the hyperfine splitting to drive transitions between the ground states. Thus, atoms receive a large velocity kick of ~1 cm/s while maintaining coherence in the ground states. This is able to separate atomic wavepackets far beyond their coherence length.

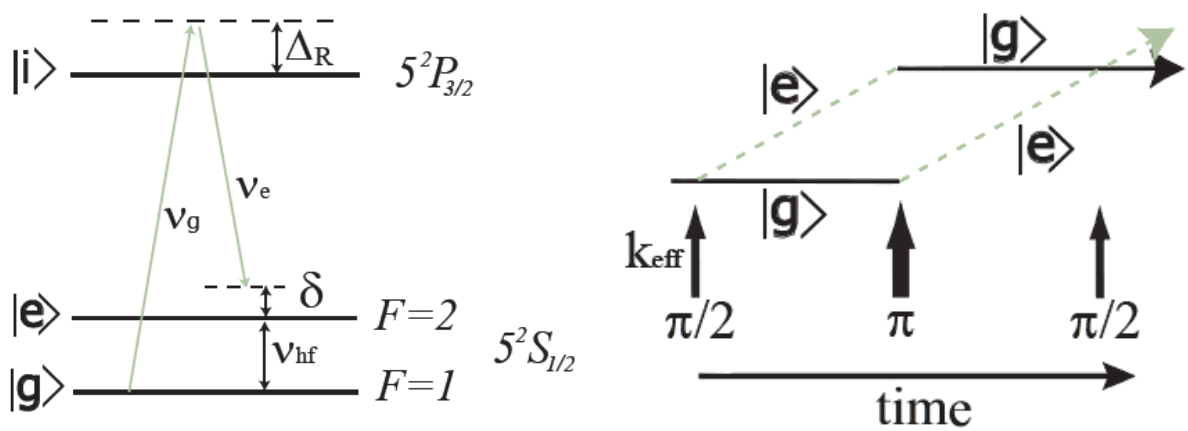

Figure 6. Left: A pair of laser beams detuned by the hyperfine resonance, ν_{hf}, couples the ground states of the atom, forming a stimulated Raman Transition. Right: A π/2 – π – π/2 pulse sequence with Raman beams forms an interferometer in space.

By using a pair of counter-propagating beams, also known as a Doppler-sensitive configuration, it is possible to entangle the momentum degree of freedom of an atom with its internal state.

One application of Doppler-sensitive Raman transitions is realized through atom interferometry [6]. Suppose an atom is prepared in the ground state, $|g\rangle$, a $\pi/2$ pulse generates an equal superposition of $|g\rangle$ and $|e\rangle$. However, the excited state receives an additional velocity recoil of $\hbar k/m \approx 1$ cm/s. The wavepackets separate for some time T, after which a π pulse inverts the atomic populations and causes the wavepackets to converge. A final $\pi/2$ pulse recombines the wavepackets, and a measurement of the populations in $|g\rangle$ and $|e\rangle$ is made. At each pulse, the light field imprints its phase onto the atoms. The net phase shift is given by $\Delta\phi = gkT^2$, where g is the acceleration experienced by the atoms. The wavenumber, k, is locked to an atomic resonance, and is thus known to a high precision. Similarly, T is based on a precise timing interval. Thus, a precise measurement of the phase results in a highly sensitive measurement of acceleration. With $\delta\phi = 3.1\ \mathrm{mrad}/\sqrt{\mathrm{Hz}}$ of phase noise and an interrogation time of T = 43 ms, atom interferometers have been able to measure accelerations at $\delta g = 4.9\ \mathrm{ng}/\sqrt{\mathrm{Hz}}$ [7]. This high sensitivity has a potentially wide application space, including seismic sensing and inertial navigation.

3.1 Pulse Efficiency Limitations

The ultimate sensitivity of an atom interferometer accelerometer is limited by the phase readout, $\Delta\phi$. However, approaching the shot-noise limit is difficult in such a system due to various systematic effects which limit the contrast of the final signal. One such limitation is pulse efficiency, where a π pulse is unable to completely transfer population to the other state. This causes "leakage" in the atom interferometer, where extra paths are generated and are unable to converge to the final measurement. Due to a total rotation of 2π in the interferometer, as a simple approximation, a π pulse efficiency of $\mathcal{E}$ corresponds to a sensitivity loss of $\mathcal{E}^2$. See Fig. 7 for experimental data demonstrating limited pulse efficiency in our previous MOT apparatus.

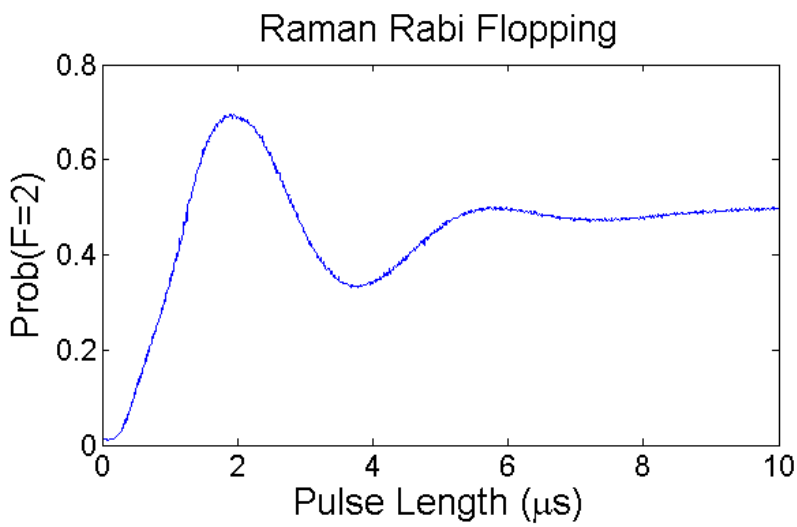

Figure 7. Sample of experimental results for Raman Rabi flopping. The observed π pulse efficiency is 70%.

Multiple effects contribute to this loss. For example, the velocity distribution of the atoms results in a Doppler shift resulting in different resonance conditions for each atom. Additionally, the spread in position results in each atom sampling a different part of the Raman beam, resulting in each atom observing a different Rabi frequency. We ran simulations of Raman dynamics assuming atoms with position and velocity distributions (Fig. 8).

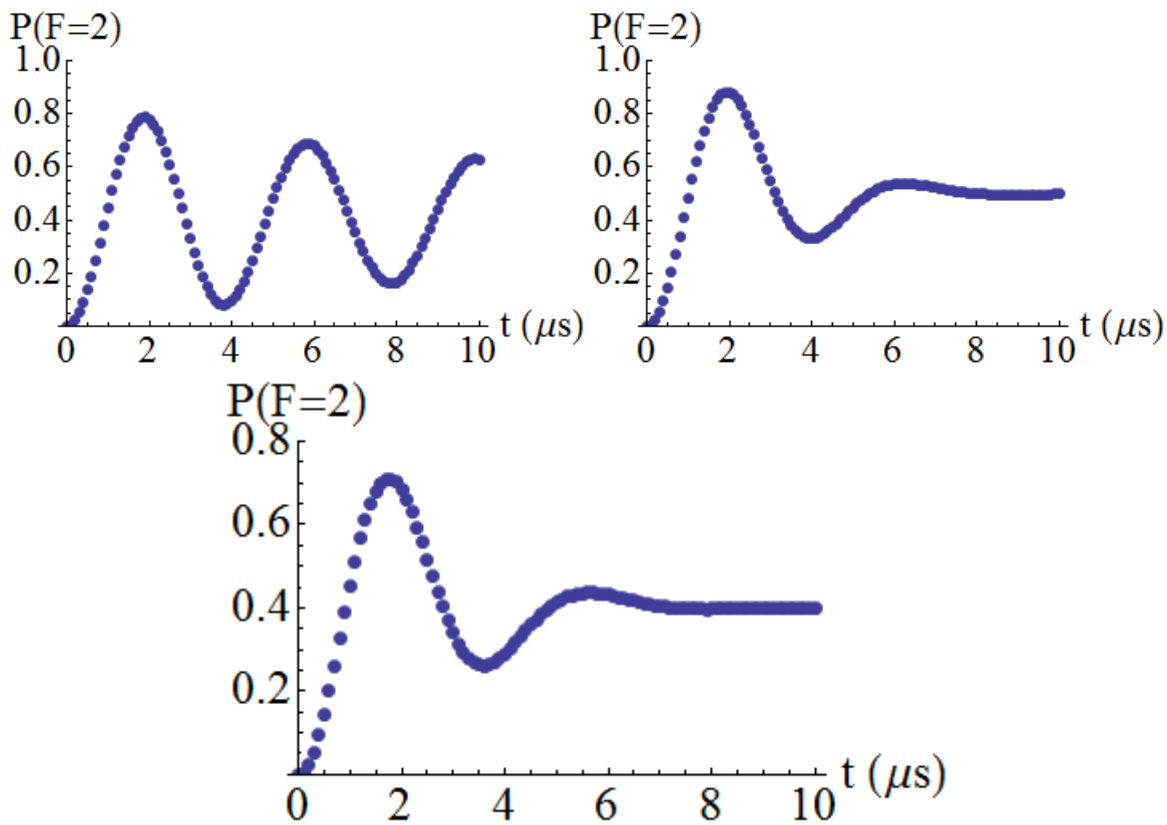

Figure 8. Simulated Raman Rabi flopping. Left: 30 μK atomic sample and homogenous Raman beam intensity. Right: Hypothetical 0K atomic sample and Raman beam is twice the diameter of the sample. Bottom: A combination of the two systematic effects.

The temperature distribution contributes to the loss of efficiency. Given a sufficiently powerful Raman beam, the velocity class addressed by the beams can be made sufficiently wide to address a large majority of atoms in the ensemble.

The dominating effect is due to variations in Rabi frequency from spatial extent of the ensemble over the size of the Raman beam. Summing over a distribution of Rabi frequencies results in a mean Rabi frequency with limited transfer efficiency. Thus, it is necessary to have a large Raman beam relative to the size of the atomic ensemble. The intensity distribution of the Raman beam may be further contaminated by the optics of the vacuum cell. Thus, although the Raman beam is sufficiently large relative to the atomic sample, fringing of the beams cause an intensity distribution across the ensemble, resulting in a reduced pulse efficiency. A combination of these two effects results in Rabi flopping similar to Fig. 7. In order to obtain and surpass the SQL, it will be necessary to have a large, powerful Raman beam with a smooth wavefront to achieve pulse efficiencies higher than 99%.

3.2 Enhanced Sensitivity

The typical $\pi/2 - \pi - \pi/2$ sequence results in sensitivity proportional to the square of interrogation time, T. The most direct way to improve sensitivity is to increase this time.

However, there are systematic consequences such as a spatially expanding atomic ensemble due to finite temperature. An alternative is to add pairs of π pulses to increase the area of the interferometer [8]. However, pulses don't perfectly transfer population as seen in the previous section. Thus, for each pulse efficiency there is an optimal number of pulses which will give the highest sensitivity. Results of the calculation are shown in Fig. 9.

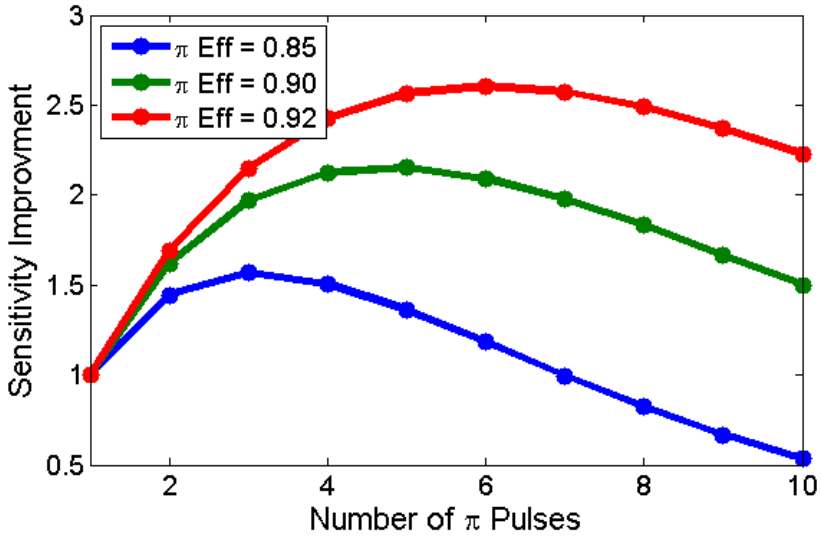

Figure 9. Plot of sensitivity vs number of additional pulses. For each π pulse efficiency, there is an optimal number of pulses.

Additionally, we can plot the optimal sensitivity as a function of pulse efficiency (Fig. 10). To see even a minor improvement in sensitivity, a pulse efficiency of 77% is required. Significant sensitivity improvements from multi-pulse techniques require >90% pulse efficiency.

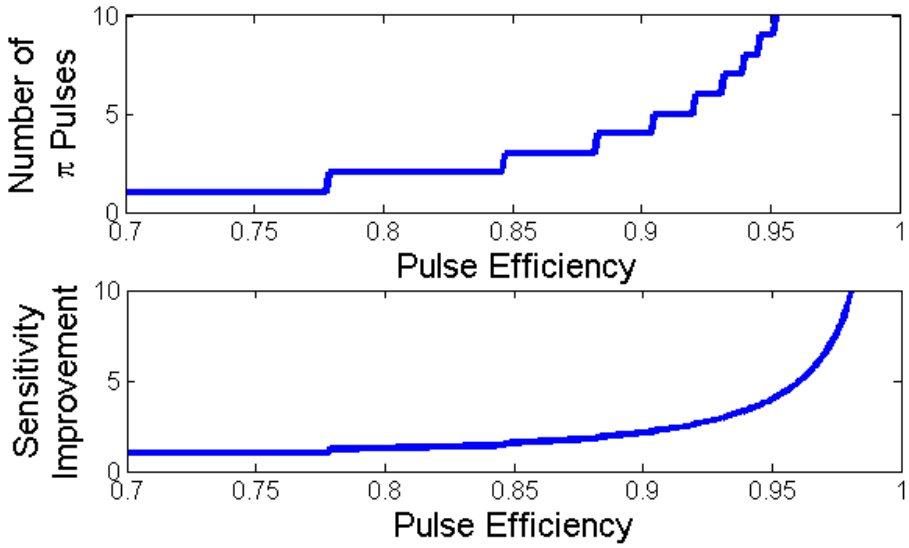

Figure 10. Top: Optimal number of pulses for a given efficiency. Bottom: Resulting sensitivity, given efficiency ε, using the number of pulses derived from top figure.

3.3 Raman Fringes

We performed a Doppler-sensitive interferometer with T = 3.5 ms at 100 Hz. Experimental data are shown in Fig. 11. The observed SNR is 30, far lower than the theoretical prediction for 10^5 atoms. There are two major contributions to this. First, the imperfect π pulse efficiency leads to a loss of contrast, corresponding to a loss of approximately 200 in SNR. Secondly, the method used to generate the Raman beams results in additional phase noise, which is then imprinted onto the atomic ensemble. This method uses two independent injection locked lasers, which is susceptible to variations in the path lengths, and therefore phase, of the two beams at the atomic sample. This generates an additional 25 mrad of phase noise on the lasers. These systematic effects must be mitigated before a true assessment of surpassing the SQL may be made.

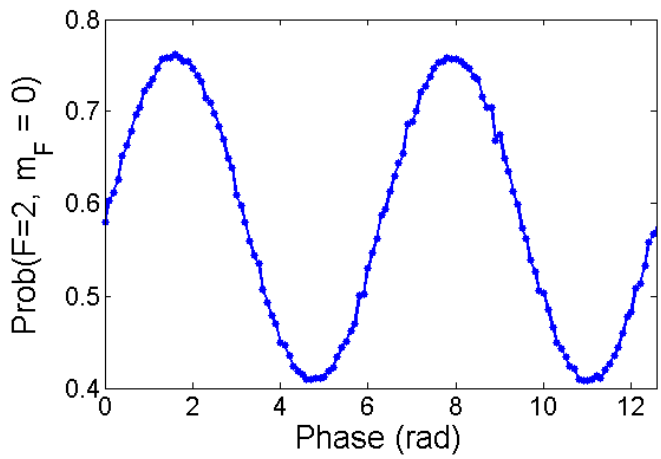

Figure 11. Fringes from a Doppler-sensitive interferometer. The phase noise corresponds to an SNR of 30.

4. THEORITICAL EXPLORATION OF SPIN SQUEEZING

Non-interacting atoms are subject to the Standard Quantum Limit, which places a lower bound for noise on the system given by SNR $= \sqrt{N}$. Through the use of a highly entangled ensemble of atoms, it's possible to relax this bound to the Heisenberg Limit given by SNR = N. For large atomic ensembles this could improve sensitivities by many orders of magnitude. However, in practice spin squeezing has only been achieved in limited systems, and has only been demonstrated slightly below the SQL and far from the Heisenberg limit. Our goal in this section is to evaluate various methods to obtain spin squeezing, and evaluate a path towards squeezing in a metrologically relevant system.

4.1 Theory

Consider a quantum spin given by $\boldsymbol{J} = (J_x,\ J_y,\ J_z)$. The Heisenberg uncertainty principle places a lower bound of the uncertainty of a measurement on such a system, given by

$$\Delta J_x \Delta J_y \geq \frac{|\langle J_z \rangle|}{2}.$$

However, there is no restriction on $\Delta J_x, \Delta J_y$ individually; the bound only applies to the product. In the case of a coherent spin state, $\Delta J_x = \Delta J_y$. In Fig. 12, this is represented by the left image showing noise evenly distributed between J_x and J_y. However, by preparing a spin-squeezed state, it is possible to increase noise in one degree of freedom (J_x) while lowering the noise on the other (J_y). Then, a measurement on J_y would result in noise less than the SQL. If J_y represents a metrologically relevant quantity, then a Heisenberg limited measurement can be approached in the limit of stronger squeezing.

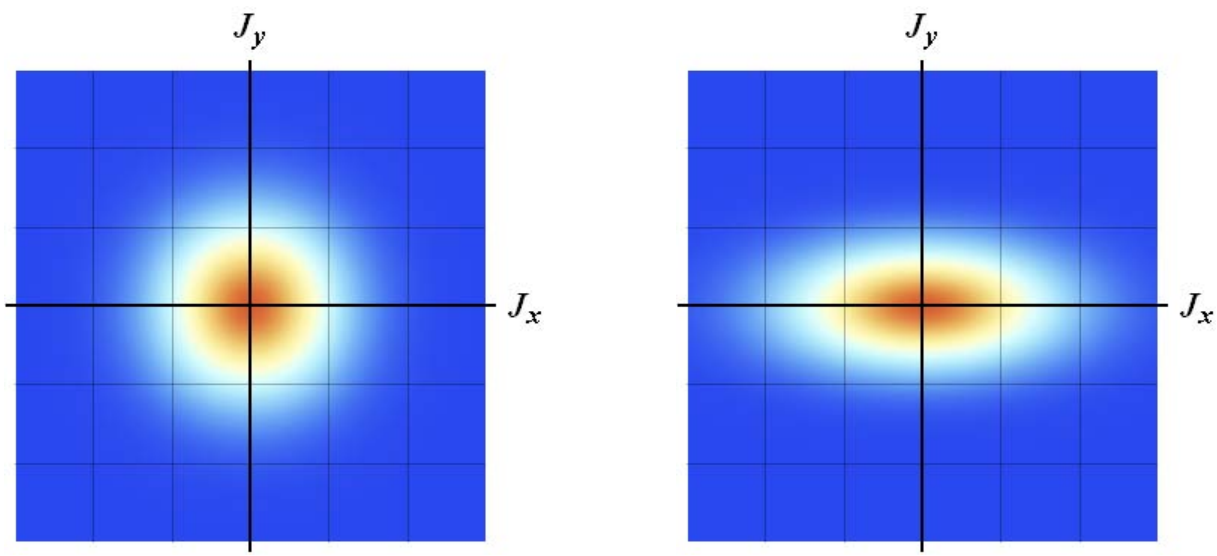

Figure 12. Left: Spin coherent state in a quantum-limited regime. Right: Coherent state squeezed along J_y.

4.2 Application to Atom Interferometry

The primary methods used to generate spin squeezing in an atomic ensemble include spin squeezing by atomic interactions, mapping squeezed light onto an ensemble, or by quantum non-demolition measurement. The first of these methods is likely infeasible in an atom interferometer since it is depending on atomic collisions, which do not allow the atoms to have a free trajectory as required by an interferometer to measure acceleration. We will consider an application of the other two methods.

4.2.1 Spin Squeezing by Atomic Interactions and Atom-Light Mapping

One technique to produce spin squeezing utilizes various atom-atom interactions to create nonlinear quantum states. Depending on the nature of the interaction and associated parameters, a controllable amount of squeezing is exhibited in one component of the ensemble spin vector, usually denoted as J_z. Due to the generally weak nature of spin interactions, the atoms must be in close proximity to one another for a significant amount of time. This generally implies the use of a Bose-Einstein Condensate (BEC).

In 2010 an atom interferometer using a spin squeezed sample of 87Rb atoms in a BEC state was demonstrated [9]. The interactions between atoms were generated using a Feshbach resonance to produce the spin squeezed state. Figure 13(a) relates the ensemble state of the atoms on the Bloch sphere to the interferometric sequence. First, a coherent spin state is produced consisting of all atoms in one of the two ground states. A complicated nonlinear pulse sequence stands in for the usual $\pi/2$ pulse and produces a spin entangled ensemble squeezed in the J_y direction and elongated in the $J_z$direction. The ensemble then undergoes free evolution, mirror (π pulse) and beamsplitter pulses. The last pulse rotates the state such that the squeezed dimension is in the J_z direction. The population difference between the two ground states maps to the fractional population in the J_z component. Measuring this population difference as a function of relative phase produces a Ramsey fringe, as seen in Figure 13(b). A close up of the mid-fringe region with error bars relates how the phase error of the experiment using squeezed states compares to the experiment without an input squeezed state. The authors report a 15% phase uncertainty decrease using the squeezed input state.

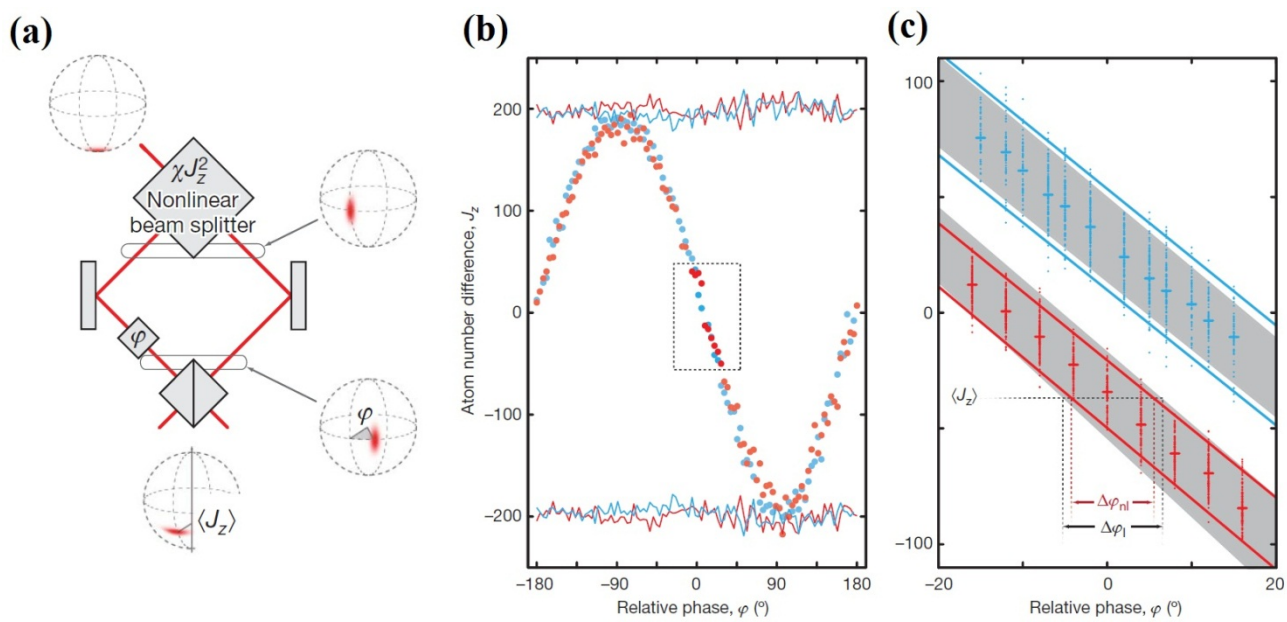

Figure 13: From [9]. (a) Evolution of an input squeezed state with an interferometer sequence. The squeezing initially produces reduced error in the J_y component, but this is transferred to the J_z component for measurement. (b) Fringes for the squeezed (red) and non-squeezed (blue) input states. (c) Uncertainties in the phases for squeezed and non-squeezed states mid-fringe.

Another method for incorporate spin squeezing into atom interferometry is through atom-light state transfer. First, phase-squeezed light is produced, often through nonlinear interaction such as optical parametric up/down conversion. This light is then incident on a cold-atom sample (not necessarily at BEC temperatures) and through a number of different interactions the squeezed nature of the light is transferred to atoms in the sample. The first experimental demonstration of this phenomenon was in 1999 [10], of which a diagram of the setup is shown in Figure 14. A classical coherent state and weak quadrature squeezed vacuum state (which has zero average amplitude but non-zero average photon number) having σ^- and σ^+ polarizations, respectively, are incident on a sample of cold Cs atoms. The beams are tuned to the $|6S_{1/2}, F = 4\rangle \rightarrow |6P_{3/2}, F = 5\rangle$ transition having frequency ω_1. The two fields interact with the $m = -1$ (coherent) and $m = +1$ (squeezed) magnetic sublevels. The atom spins become aligned with the incident light and spin entangled with one another. The ensemble is then probed with light tuned to the $|6P_{3/2}, F = 5\rangle \rightarrow |6D_{5/2}, F = 6\rangle$ transition and linearly polarized 45° to the x axis. It can be shown [8] that this leads to a spin squeezed state where the spin component in the x direction has the relation to the total spin vector F of

$$\langle F_x^2 \rangle = \frac{1}{4}\langle F \rangle.$$

This implies a spin squeezing in the x spin component of 50%, that is, spin measurements on the x component will exhibit 50% less fluctuations than they would without the incident squeezed light.

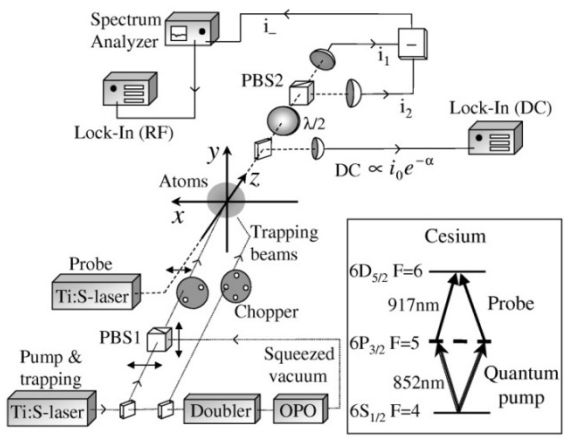

Figure 14: From [10]. Experimental setup for mapping a squeezed light state onto an ensemble of cold Cs atoms. Coherent and squeezed light is incident on the ensemble, creating a spin entangled, and spin squeezed, state. The component of the ensemble spin which is squeezed is measured via probe beam and lock-in detection methods.

This experiment was only able to demonstrate around 5% squeezing, with the reduced efficiency blamed on multilevel effects, imperfect polarizations, fluctuating ambient magnetic fields among other causes. As such it offers little improvement over classical methods and requires a host of additional equipment. Fortunately, this is one method among several to map squeezed light onto atoms. Recently at least two different schemes have been put forth to improve the mapping efficiency [11,12]. As this technique improves it could be feasible that enough will be gained from spin squeezing atoms via squeezed light to be worth the increased effort that generating squeezed light implies.

4.2.2 Spin Squeezing by Quantum Non-Demolition Measurement

A more mature and demonstrated method for achieving spin squeezing in an atomic ensemble has been demonstrated through the use of a quantum non-demolition measurement. Using this technique, spin squeezing has been demonstrated to surpass the shot noise limit in a microwave clock [13]. In this experiment, 10^5 cesium atoms were placed in a spin squeezed state. The phase of a 10 µs Ramsey microwave interferometer was read with a sensitivity better than the expected value from the SQL.

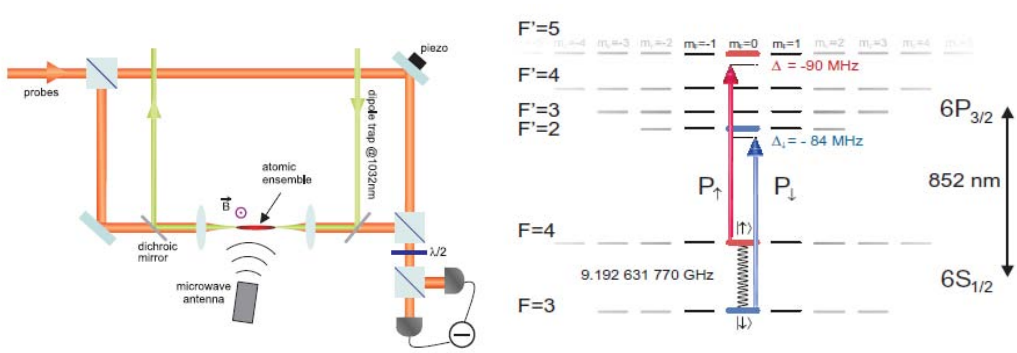

Figure 15. From [13]. Left: Interferometer used to detect phase shifts in the probe beam. Right: Energy level diagram of the two-color probe beam.

Fig. 15 illustrates the experimental setup used to generate the QND pulse. The probe beam is sent through two arms of an interferometer, with the atomic sample in the path of one arm. The probe beam consists of two frequencies, tuned such that the coupling constants for each transition are equal. The result is a state-dependent phase shift imprinted on the light and read by the interferometer. The phase shift imprinted onto the light field is given by

$$\phi = \frac{\delta n}{\beta n} + \chi \Delta N + \Delta \chi N_A,$$

where the first term represents photonic shot noise, χ and $\Delta\chi$ are derived from coupling constants, ΔN is the population difference between hyperfine levels, and N_A is the total number of atoms. This measurement is able to maintain the superposition of an atomic state since only information about the sum of population difference and total population is acquired. However, the state does undergo a "partial collapse", where the uncertainty along J_z is diminished. Thus, by using information obtained from the first measurement, any subsequent measurement should result in a lower measurement variance.

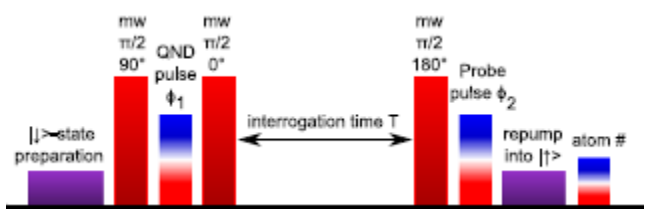

Figure 16. From [13]. Experimental sequence used to surpass the SQL by QND measurement.

The experiment proceeds as shown in Fig. 16. The state is prepared in a superposition of the hyperfine energy levels. A QND pulse measures the quantity ϕ_1 without destroying the superposition, thus generating the squeezed state. Note that in order to actually be below the SQL, the result ϕ_1 must be maintained. The Ramsey microwave interferometer is then applied with some interrogation time *T*. A second QND pulse measures ϕ_2 after the interrogation. The atoms are repumped, and a total population measure is made, which may be destructive. While the variances of ϕ_1 and ϕ_2 independently respect the SQL, the variance of $\phi_2 - \phi_1$ was found to be below the SQL by -1.1 dB at T = 10 μs. Systematic limitations prevented exceeding the SQL for longer interrogation times.

There were some limitations to the experiment which have to be overcome for operation in an atom interferometer. The primary limitation was the use of an optical dipole trap to keep the atoms confined during state preparation, interrogation, and detection. The trap was necessary to attain high optical densities required for the QND measurement, as well as to limit atomic motion so that atoms are addressed evenly by the probe beam. Therefore, the apparatus would be unable to perform inertially free measurements. Secondly, as a consequence of the light used to maintain the dipole trap, the atoms are subject to a position-dependent ac-Stark shift. This causes dephasing for longer interrogation times, which are required for high-sensitivity atom interferometers.

Instead, we will consider a similar experiment where the dipole trap is turned off immediately after the QND preparation, and turned on immediately before the QND detection. Then, the atoms are inertially free for the interrogation [14]. Despite the retrapping, the inertial result is stored in the atomic state, so there is no loss of inertial information. The interrogation time of the interferometer is limited by how efficiently we can recapture atoms into the trap. The Rayleigh range for a dipole trap, which defines the size of the trap on the longitudinal axis, is given by,

$$z_R = \frac{\pi \omega_0^2}{\lambda}$$

Where λ is the wavelength of the trapping light and ω_0 is the beam waist. Using experimental parameters from [13], $\lambda = 1032$ nm and $\omega_0 = 20$ μm, we have $z_R = 1.2$ mm. Assuming the atoms are accelerating under gravity, this corresponds to a maximal interrogation time of 15.8 ms. However, the limiting factor is likely to be thermal expansion of the atomic ensemble. Since the ensemble expands in all directions, we have to consider the trap size to be limited by ω_0. We carried out a Monte Carlo simulation of recapture efficiency assuming these trap parameters with T = 1 μK, which can be reached with light-base cooling techniques. Results are shown in Fig. 17. The simulation demonstrates minimal atom loss up to 1.5 ms of flight.

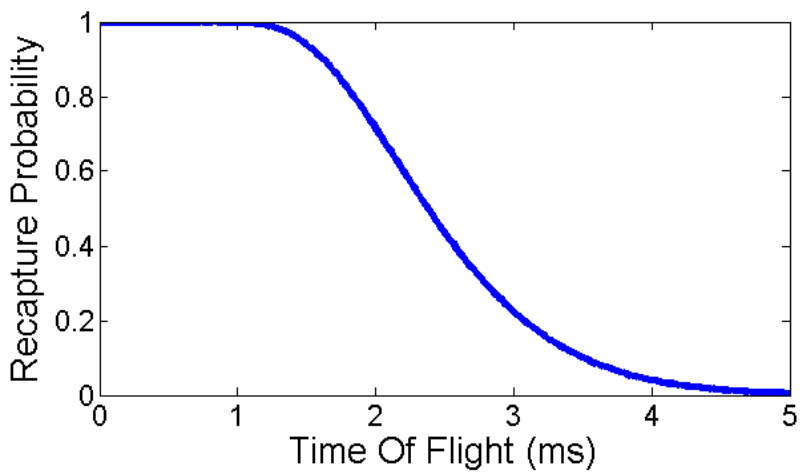

Figure 17. Simulation used to model recapture efficiency vs time of flight from a dipole trap. Parameters used were ω_0 = 20 μm, T = 1 μK.

If we choose a short interrogation time, we retain most of the atoms but lose sensitivity due to the T^2 scaling of the interferometer. For long interrogation times, we have sensitivity but observe increased phase noise due to the loss of atoms. There is an optimal interrogation duration based on whether the phase obeys the standard quantum limit or Heisenberg limit. Results of the calculation are shown in Fig. 18.

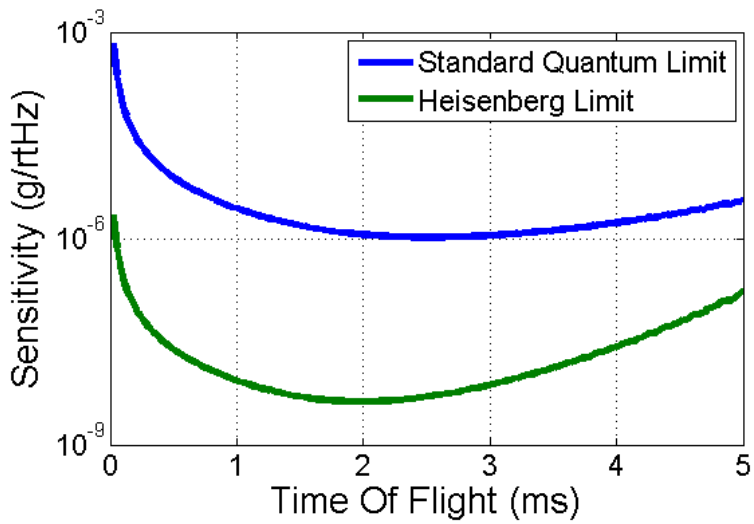

Figure 18. Optimal sensitivity of an atom interferometer out of a dipole trap using SQL limited detection vs Heisenberg limited detection.

Under the standard quantum limit, the optimal sensitivity is found to be ~1 $\mu g/\sqrt{Hz}$ at 2.5 ms or 400 Hz. The sensitivity under the Heisenberg limit is found to be ~4 $ng/\sqrt{Hz}$ at 500 Hz, over two orders of magnitude better.

While approaching the Heisenberg limit is appealing, there exist several limitations which make it difficult in practice. First and foremost, to achieve strong spin squeezing by QND, a high optical depth is required. In the case of [12], the optical depth was approximately 10 with an atomic density of 3×10^{10} atoms/cm^3, which resulted in a squeezing of -1.1 dB. To achieve the -24 dB of squeezing represented by the Heisenberg limit, the optical depth would have to be increased by two to three orders of magnitude. This would require a tightly confined atomic ensemble and detection beam, which can be achieved with an atomic density of approximately 10^{13} atoms/cm^3. While this is difficult to achieve in a dipole trap or optical lattice, it is readily accomplished in a BEC. However, BECs are subject to atom-atom collisions which impact the fidelity of the measurement. Despite this, there is work being performed towards a ballistic atom interferometer with a BEC [15].

5. CONCLUSIONS

Quantum metrology has demonstrated promise in a wide variety of fields ranging from precise timing to inertial navigation. These systems are subject to a fundamental limit to sensitivity known as the standard quantum limit, where the SNR is limited to $\sqrt{N}$, where N is the number of atoms. Using more advanced techniques, it is possible to achieve what is known as the Heisenberg limit, where the SNR limit is N. We characterized sources of noise leading to the SQL, as well as explored techniques to surpass this in hopes of achieving Heisenberg limited sensitivity in a practical system.

Our initial investigations focused on reaching the SQL in microwave systems. In the case of a cold-atom system, we were able to characterize and mitigate sources of noise and were thus able to approach the SQL. Additionally, we created an apparatus with which we could evaluate microwave transitions in room temperature vapor cells.

We continued our studies with a theoretical analysis of stimulated Raman transitions, which have potential applications in inertial navigation systems. We were able to identify sources of low pulse efficiency as well as model sensitivity enhancements through multi-pulse techniques. It is clear that advancing traditional techniques is required before surpassing the SQL may be realized.

One method to surpass the SQL is through the use of spin squeezing, which has a theoretical sensitivity bound given by the Heisenberg limit. We evaluated various methods of spin squeezing and performed a theoretical analysis of surpassing the SQL with a novel dipole trap based atom interferometer.

6. REFERENCES

1. E. L. Raab, M. Prentiss, A. Cable, S. Chu, D. E. Pritchard. *Trapping of neutral Sodium atoms with radiation pressure*, Physical Review Letters, Volume 59, 1987.
2. H. Metcalf, P. van der Straten, *Laser Cooling and Trapping*, Springer, NYC, 1999.
3. H. McGuinness, A. Rakholia, G. Biedermann, *High data-rate atom interferometer for measuring acceleration*, APL, Volume 100, Number 1, January 2012.
4. S. J. Seltzer, et al., *Investigation of Anti-Relaxation Coatings for Alkali-Metal Vapor Cells Using Surface Science Techniques*, J. Chem. Phys., Volume 133, 2010.
5. K. Moler, D. S. Weiss, M. Kasevich, S. Chu., *Theoretical analysis of velocity-selective Raman Transitions*, Physical Review A, Volume 45, Number 1, January 1992.
6. M. Kasevich, S. Chu, *Atom Interferometry Using Stimulated Raman Transitions*, Physical Review Letters, Volume 67, Number 2, July 1991.
7. G. Biedermann, Gravity Tests, *Differential Accelerometry and Interleaved Clocks with Cold Atom Interferometers*, Ph.D. Thesis, Stanford University, November 2007.
8. J. M. McGuirk, M. J. Snadden, M. A. Kasevich, *Large Area Light-Pulse Atom Interferometry*, Phys. Rev. Letters, Volume 85, Number 21, November 2000.
9. C. Gross, T. Zibold, E. Nicklas, J. Esteve, M. K. Oberthaler, *Nonlinear atom interferometer surpasses classical precision limit*, Nature Letters, Volume 464, 2010.
10. J. Hald, J. L. Sorensen, C. Schori, E. S. Polzik, *Spin Squeezed Atoms: A Macroscopic Entangled Ensemble Created by Light*, Phys. Rev. Letters, Volume 83, Number 7, August 1999.
11. M. E. Tasgin, P, Meystre, *Spin squeezing with coherent light via entanglement swapping*, Phys. Rev. A, Volume 83, 2011.
12. M. Takeuchi, S. Ichihara, T. Takano, M. Kumakura, T. Yabuzaki, Y. Takahashi, *Spin squeezing via one-axis twisting with coherent light*, Phys. Rev. Letters, Volume 94, 2005.
13. A. Louchet-Chauvet, et. al., *Entanglement-assisted atomic clock beyond the projection noise limit*, New Journal of Physics, Volume 12, 2010.
14. L. P. Parazzoli, A. M. Hankin, G. W. Biedermann, *Observation of Free-Space Single-Atom Matterwave Interference*, arXiv:1208.4898, August 2012.
15. J. Hogan, *Gravitational Wave Detection with Atom Interferometry*, 8th International LISA Symposium, Stanford University, July 2010.

DISTRIBUTION

1	MS0899	Technical Library	9536 (electronic copy)
1	MS0359	D. Chavez, LDRD Office	1911

Sandia National Laboratories